

LIFETIME ASPECTS OF WEARABLE ELECTRONICS

Hans de Vries

Philips Research Laboratories, Eindhoven, The Netherlands

Abstract. *In the course of two European projects the endurance behavior of stretchable electronic substrates and of electronic textiles was investigated. The results have to a large extent been published already. In this work new analyses to the earlier results are presented. Straightforward analytical approaches are used to describe fatigue under cyclic mechanical loading in the two technologies. For stretchable substrates the actual plastic strain upon stretching could be qualitatively evaluated to replace the engineering strain. For the textile-based substrates the bending strain was estimated. Additionally, there are sub-categories within each technology which perform differently and apparently show percolation behavior.*

Key words: *stretchable electronic, electronic textile, endurance test, cyclic mechanical loading, fatigue, percolation*

1. INTRODUCTION

During the last decade or perhaps even longer the notions of wearable electronics and smart textiles have received ever more attention. The main justification for this development is the possibility to make electronic applications that are conformable around complex shapes. One can think of monitoring human body functions where small signals need to be measured and thus the devices must be placed close to or on the skin. The application areas are amongst others in health care, wellness and leisure. But one has also a larger freedom of design in consumer and professional products, for instance lighting and automotive.

In this contribution the endurance behavior of the abovementioned technologies is addressed.

Quite understandably, initially research and development organizations have spent most effort to the study and development of the application areas and the technologies. As for stretchable substrates with conducting tracks and components, the first investigations are from Princeton University, Lawrence Livermore National Laboratories, and John Hopkins University (see references in [1]). Here, we refer to the European project STELLA* where three technologies were investigated and demonstrator products were made [1, 2, 3]. Textile-based technologies and applications were the subject of the European project

Received September 25, 2014

Corresponding author: Hans de Vries

Philips Research Laboratories, High Tech Campus 34, 5656AE Eindhoven, The Netherlands

(e-mail: j.w.c.de.vries@philips.com)

* STELLA: *Stretchable electronics for large area applications*. IST-028026, 2006–2010.

PLACE-it[†]. Recently, an extensive review has been published on the history of smart textiles, trends and identifying the important challenges such as the manufacturing technologies and the robustness of the products [4]. Of course, much more has been published on stretchable and textile-based electronics, but it is not the purpose of this paper to give a full account of the literature.

An important factor that needs attention before products are introduced on the market is the reliability and the lifetime. Since reliability is defined as ‘the ability / probability of a product to fulfill its intended function, under specified loading conditions, during a specified period of time’, the reliability and the lifetime requirements depend on the application. One thus has to make an inventory of the relevant stress factors that the product will be subjected to, and test them accordingly. Especially when new applications, or new technologies, or new materials, or a combination of these are developed, one might encounter new stress conditions which ask for new test strategies.

Two examples may serve as illustration. Suppose one designs an activity monitor for para medical usage or for athletes (such as to measure heartbeat, respiration frequency et cetera). The device will stretch about 5% when pulling it over the wrist; in actual use the stretch is less. This will be done ten to twenty times daily for say three hundred days per year. With a desired lifetime of three years, the product should endure up to ten thousand stretch cycles of 5%. The second case is a textile-based device that will be tightly wrapped around a limb or the body – a device for instance that is meant for skin treatments (light therapy). Because in the warp and weft directions a textile is only limited stretchable (a few percent perhaps) the most important stress type is that of bending each time the device is applied. With a required lifetime of three years, the product must endure several thousand bending cycles. Of course, this will also depend on the bending radius.

A special feature of wearable electronic products is washability. This was also touched upon in the two referenced European projects, but indeed the scope was comparatively limited, and as far as the author is aware no results were published. Apart from the fluids and detergents, obviously various mechanical stresses will be imposed on the products: bending, folding, rolling, and shock impacts.

To summarize, the introduction of stretchable and textile-based electronic products goes hand in hand with additional factors that have influence on the reliability and the lifetime of these products. It will be clear that the conventional stress factors, such as temperature and humidity, still apply and must be tested for.

This leads to the actual purpose of the paper, which is to address the particularities of wearable electronics that relate to reliability and lifetime. All data come from the two European projects that were referred to earlier. Often a dedicated test setup had to be designed to investigate the failure modes. A couple of results on endurance tests have been published for stretchable electronics [5, 6] and structures made with woven and non-woven textile [7, 8]. Sometimes, a model description for the failure mechanism could be included. It is worth to review these earlier studies and try to further explore the possibilities of modeling the failure mechanisms. These will be rather simple models, but they are only meant to shed light on the underlying physics. Thus we hope to encourage other researchers to continue in this field.

[†] PLACE-it: *Platform for large area conformable electronics by integration*. IST-0248048, 2010–2013.

The main subject is the fatigue lifetime modeling of the two technologies in general. However, within each of these two there is a category which cannot be related to fatigue. Instead, there are indications that the behavior of these categories should be explained in terms of percolation theory.

The paper is organized as follows. In the second chapter the samples fabricated with the various technologies are briefly introduced. Also the test methods and the test results are presented, including the essential results of the failure analyses. Fatigue lifetime analyses are the subject of the third chapter. The above mentioned special categories will be discussed in chapter four. Finally, a summary and outlook are formulated.

2. TEST STRUCTURES, TEST METHODS, AND TEST RESULTS

As was mentioned, nearly all test structures, methods and results have been published already, and thus we will give only a brief description in this chapter. Further details can be found in the referenced literature. At the end of this chapter a compilation of the available test data will be made, which will be further analyzed and discussed in the next chapter.

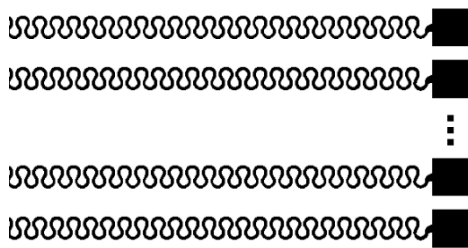


Fig. 1 Meander structure of stretchable copper board and stretchable molded interconnect technologies [5].

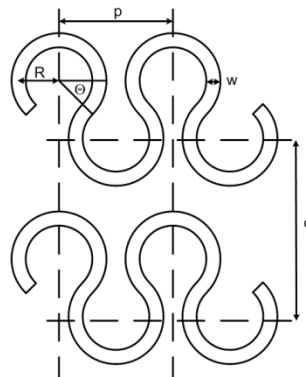


Fig. 2 Design of meander and definition of parameters [5, 9, 11].

2.1. Stretchable technology

For each of the three stretchable technologies basically the same test structures were used [5]. These have a meander-shaped conductor incorporated in or on the stretchable substrate. A meander-like structure allows for larger deformations of the metal conductor as it acts as a kind of spring [9]. Other shapes, which have a spring-like feature in common, have been proposed and studied as well, see e.g. [10].

The second technology is called stretchable molded interconnection (SMI) and uses polydimethylsiloxane structures (PDMS, Sylgard 186 of Dow Corning) [3]. Here, the copper tracks have a thickness of 18 μm . The total thickness of the substrate is 1 mm.

A typical layout of the samples for both technologies is shown in Figure 1. The influence of the shape of the meander – the angle (Θ), radius (R), pitch (p), and width (w), see Figure 2 – on the mechanical properties [9, 11] and the endurance behavior [12, 13] has been investigated.

The third technology is called stretchable polymer board (SPB) and one applies screen printing of a conductive paste on a polyurethane micro fiber carrier non-woven material [2]. The paste consists of a thermoplastic polyurethane matrix filled with silver-coated flakes. In this case a horseshoe shape of track was made (for this case, in Figure 2 the angle $\Theta = 0$). The substrates have a thickness of about 0.27 mm. We will present and discuss the results in chapter 4.

2.2. Electronic textile

Two basic types of textile samples were manufactured for the endurance tests. One type is made by weaving conductive yarns into a textile, mostly parallel to the warp direction [4, 7]. Since light therapy is considered as a possible application, light emitting diodes (LEDs) are mounted on the textile on positions where the conductive yarn lies on top of the weave, the so-called floats.

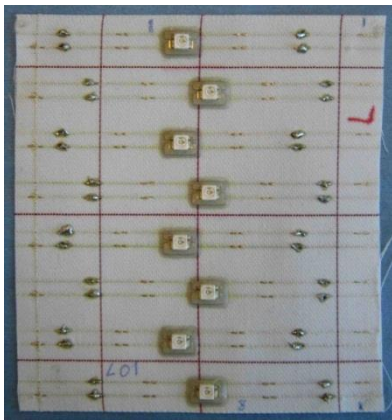


Fig. 3 Woven test sample with rows of LEDs [7]. The globtop is visible as the brown ring around the LEDs. The conductive yarns are in the warp direction (left-right).

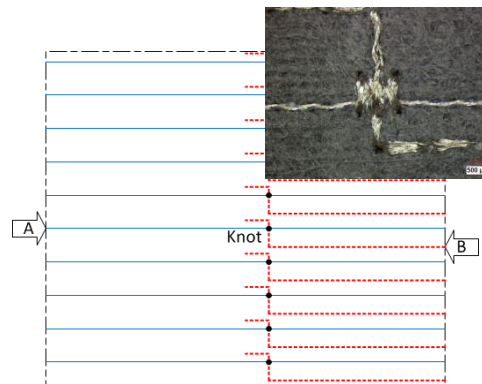


Fig. 4 Layout of non-woven test structure of combined stitched (red dashed lines) and embroidered conductive yarns (blue solid lines) and interconnection [8]. (black dot, see insert). The resistance is measured between A and B.

In Figure 3 an example of a textile with LEDs is depicted. The LEDs are electrically connected to the conductive yarns with conductive adhesive paste and this connection is reinforced by globtop around the LED. Typical dimensions of the textile are $85 \times 100 \text{ mm}^2$. The weave is characterized by the thickness of the cotton wire which is given by the dtex-number (mass in grams of 10,000 meter of wire) and the pitch of the weave, given in

picks per centimeter. The conductive yarn consists of 20 silver-clad copper filaments of $40\ \mu\text{m}$ thickness. The bundle has a twist of about 240 turns per meter.

The other type of textile test sample is made from non-woven material of about $0.6\ \text{mm}$ thickness and size of $80 \times 150\ \text{mm}^2$. Conductive yarns are bundles of 34 polyamide filaments which are coated with about $1\ \mu\text{m}$ silver. Two different techniques were used to attach these yarns to the substrate. One is by stitching with a sewing machine. In this case an upper and an under yarn – both conductive – are stitched together. Alternatively, the conductive yarn is embroidered to the top of the substrate by a separate, non-conductive yarn. This is called *soutache*. In the test samples both techniques were combined and the two yarns were connected by a knot as shown schematically in Figure 4. One can also connect two similar yarns in this way; the essential point is to use existing methods of applying yarns and making electrical interconnections. The insert shows a detail of such interconnection. The resistance was monitored between the points A and B. For further information, see [8]. The results will be discussed separately in chapter 4.

2.3. Test methods

From the introduction it will have become clear that the relevant type of stress is repeated bending or stretching. Thus, test setups are needed to provide such deformation in a cyclic manner to the test structures. The stretchable were mounted in test machines – either commercially available or home built – and subjected to stretching cycles of up to 20% for SCB- and even higher for SMI-technology, and 5% for the SPB-samples [5, 14]. Care was taken not to stretch the samples too close to the limit of maximum elongation. Simultaneously, the integrity of the metallic conductors and of the electrical interconnections was monitored in order to determine the moment of failure.

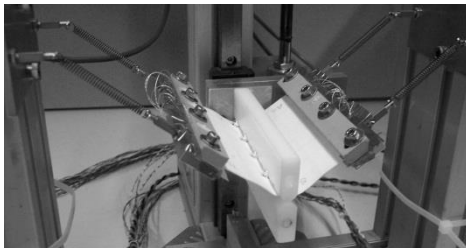


Fig. 5 Setup for cyclic bending test, showing springs to hold the textile straight, and clamp (white blocks) to move the sample up and down.

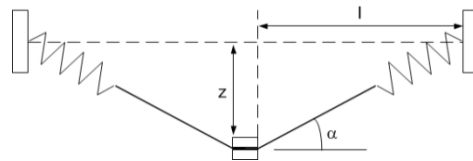


Fig. 6 Schematic of cyclic bend test with springs, and clamp moving up and down over distance (z). The half-length of the non-rigid part is given by l .

For the electronic-textile samples a dedicated bending test machine was built as described in [15]. The sample (Figure 5) is held straight by springs. The central part with the LEDs is moved down and back again, which causes the textile substrate to bend next to the row with LEDs which are rigid, see Figure 6. The current through the LEDs was recorded to observe the moment of failure in the conductive yarns or in the electrical interconnections. In the same contraption the non-woven substrates with the stitched and embroidered conductive yarns (Figure 4) were put to test. Here, the row with the knot-

type of interconnections is tested. The electrical resistance of the conductive yarns was measured.

The layout of the various test structures made it possible to do a number of measurements per sample in parallel. In most of the cases experiments were repeated, so that in the end a statistical evaluation of the failure data could be done. For that purpose Weibull-statistics were applied. The two-parameter Weibull-function is a probability distribution function described by a scale parameter (η) denoting its position and a shape parameter (β) denoting its width. The cumulative distribution function as function of time (t) is:

$$F(t) = 1 - \exp[-(t/\eta)^\beta] \quad (1)$$

Examples of failure distributions with the 95%-confidence levels are given in Figure 7 and Figure 8. The slopes of the distributions are 6.4–10 for the SCB-samples and 3.5–4.8 for the textile samples. These values indicate that accelerated test conditions were applied, leading to wear out failures.[‡]

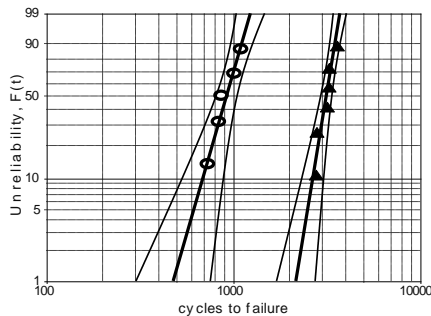


Fig. 7 Weibull failure distribution with 95%-confidence levels of SCB-samples cyclically stretched to 5% (▲) and 7.5% (○).

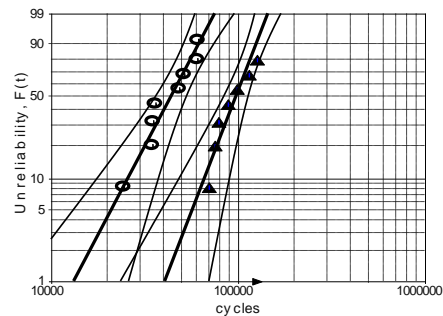


Fig. 8 Weibull-failure distributions with 95%-confidence levels of textile sample cyclically bent by displacing over 59 mm (▲) and 77 mm (○).

2.4. Test results & Failure analyses

In the following paragraphs of this section the results from the endurance tests are collected. Both the lifetime results and the failure analyses will be given. For each case – stretchable, textile – the cyclic lifetime is given as it was obtained for each test condition. This will be the elongation or engineering strain for the stretchable samples, and the displacement (z) imposed by the bending tool (see Figure 6) for the textile-based samples. The lifetime is defined as the scale parameter of the Weibull-distributions (η , see equation (1)), which is thus the time or number of cycles to 63.2% failures.

[‡] The failure rate decreases over time (t) for $\beta < 1$ (early failures), is constant for $\beta = 1$ (random failures), and increases for $\beta > 1$ (aging or wear-out failures). For severe or accelerated test conditions, β can have values well larger than two or three.

Table 1 shows the results for two of the stretchable technologies. Similar is listed in Table 2 for the textile substrates. It should be mentioned, that after 950,000 cycles to 2.6% stretch, the SMI-sample had not failed. In the same sense the textile-bending test to 35 mm displacement did not lead to complete failure, but several filaments in the bundle were broken, and so we include this result in the evaluations as were it a failure.

Table 1 Engineering strain and observed cycles to failure for the indicated stretchable technologies. The margins are the 90%-confidence levels from the failure distributions.

Technology	Strain (%)	Cycles to failure	Reference
SCB	20	150±20	5
	15	300±50	
	10	700±100	
	7,5	920±120	
	5	3200±200	
	2,5	45000±6500	
SMI	20	200±50	5
	15	500±150	
	10	2100±800	
	10	2500±800	
	7,5	3300±300	
	5	16000±6000	
	4	100000±15000	
	2.6	950000: no failure	

Table 2 Displacement (z) and observed cycles to failure for textile with indicated characteristics (dtex in grams per 10,000 meter of yarn, picks/cm in number of yarns per cm). The margins are the 90%-confidence levels from the failure distributions.

Textile	z (mm)	Cycles to failure	Reference
dtex: 76	86	25000±7000	7
picks/cm: 33	77	49000±8000	
	59	105000±20000	
	35	1500000: partial failure	

Finally, selected results from the failure analyses will be given as an illustration to reveal the failure mechanisms. This is one essential step to decide which models should be used for a description of the lifetime in the stretchable and textile substrates. In Figure 9 and Figure 10 for SCB and in Figure 11 and Figure 12 for SMI typical examples of the failure mode in the meandering Cu-tracks of the stretchable substrates are shown. From the pictures one can derive that the failure mechanism is fatigue, caused by the mechanical cycling. From the statistical analyses (see e.g. Figure 7) it followed that the cumulative distributions are near parallel to each other, which supports the conclusion that the same failure mechanism applies for all cases.

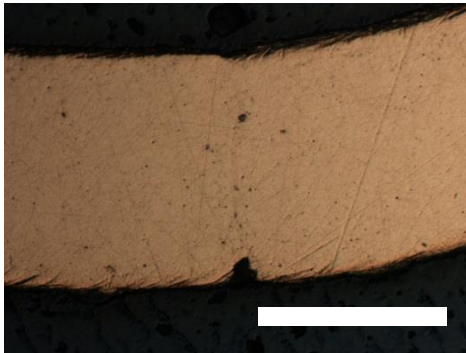


Fig. 9 SCB-sample with fatigue deformation. The scale bar is 100 μm .

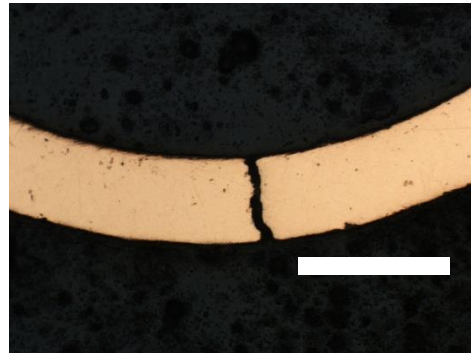


Fig. 10 SCB-sample with fatigue crack after testing to 5% stretching. The scale bar is 200 μm . From [5].

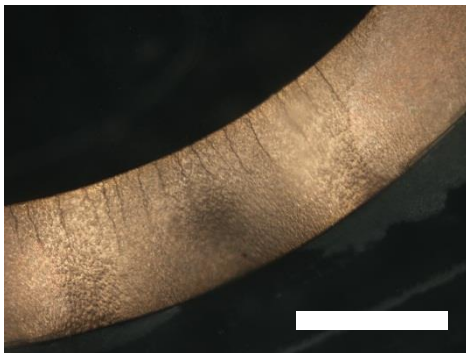


Fig. 11 Micro cracks in the Cu-track of SMI-sample after testing to 4% stretching. The scale bar is 100 μm . From [5].

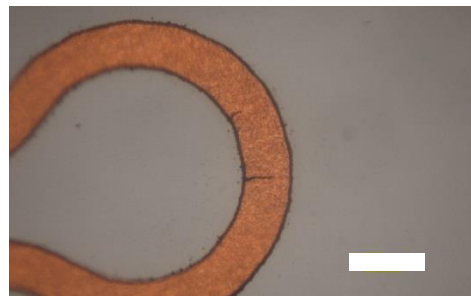


Fig. 12 Incomplete fatigue crack in the Cu-track of SMI-sample after testing to 4% stretching. The scale bar is 200 μm .

As for the textile-based technology, some results of failure analyses have been published before [7], but since these are new in comparison to the polyurethane-based stretchable technologies it is useful to elaborate a little bit more here. Figure 3 shows a typical layout of an electronic textile with rigid components (LEDs reinforced with globtop). Upon bending most of the deformation takes place at the transition from the rigid to the textile parts (see Figure 5 and Figure 6) – and this is exactly the location where failure occurs. In Figure 13 an X-ray image of a detail of the textile with LED after the cyclic bend test is shown. One can see the position where the bundles of filaments are broken. Next to this picture, Figure 14 shows an optical image of the same part where one of the two broken conductive yarns has been pulled out of the weave. The failure site coincides with the edge of the globtop. To be complete, a cross section of such a construction proves that indeed the metallic conductor breaks right outside the edge of the rigid globtop. One can see this in Figure 15 where a part of the LED is shown with its lead attached to the conductive yarn in the textile. The electrical interconnection is made with conductive

adhesive, which is a mechanically weak connection. Therefore globtop is applied which is also visible in the photo. The detail of Figure 16 reveals a crack in the Cu-filaments close to where the globtop ends. All this is evidence for fatigue as failure mechanism.

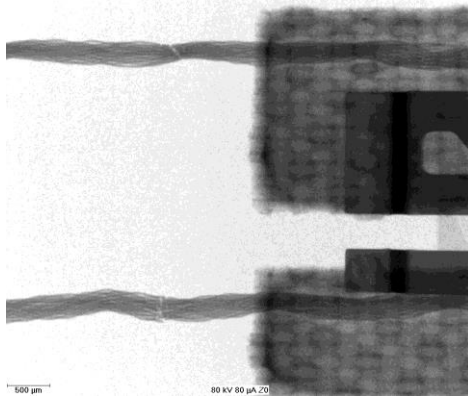


Fig. 13 X-ray image of LED-on-textile after cyclic bend test. The two conductive yarns are broken at the edge of the rigid to textile transition.

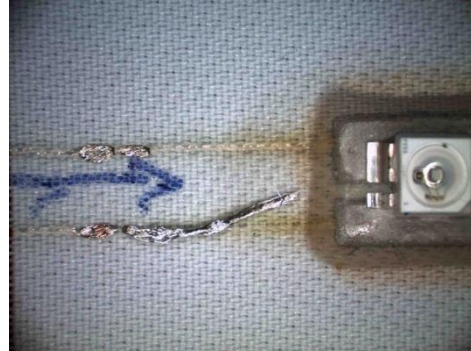


Fig. 14 Optical photo of LED-on-textile after cyclic bend test, same as in Figure 13. One of the two conductive yarns has been pulled out of the textile.

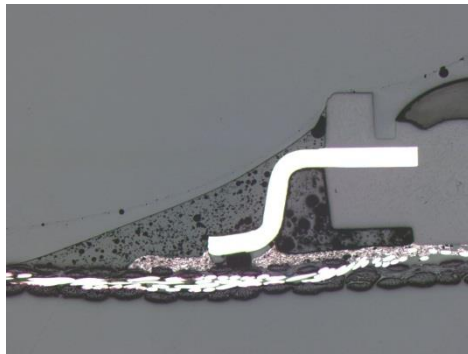


Fig. 15 Cross section of LED on textile with from top to bottom: lead / adhesive / yarn. The dark grey mass is the globtop.

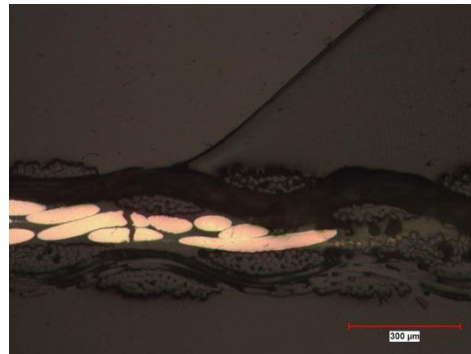


Fig. 16 Cross section showing yarn with crack close to the edge of the globtop.

The statistical analyses indicate that in all test cases the conductive yarns failed because of the same mechanism: the cumulative distributions are in parallel, as one can infer from Figure 8.

Before turning to the evaluation of the results in order to develop a model description of the failure mechanism, it may be convenient to summarize the results that were collected. Cyclic endurance tests have been carried out. Samples based on stretchable technologies were elongated to various levels until electrical failure occurred. Similarly, samples based on electronic textile were bent at different levels. The number of cycles to failure depends on the strain level. From the failure analysis it was concluded that the failure mechanism is fatigue.

3. ANALYSES & DISCUSSION

In the analyses of below chapter, first the some basic elements that relate to fatigue will be discussed. Then we will provide additional evaluations of the data that were published earlier. This leads to a close agreement with results obtained on stretchable substrates that are reported in other research.

3.1 Fatigue general

As we have discussed in the previous chapter, fatigue has been identified as the mechanism of failure. In so far as low-cycle fatigue is concerned, the well-known Manson-Coffin relation [16] is commonly used to describe the cycles to failure as function of the applied strain:

$$\frac{\Delta \varepsilon_p}{2} = \varepsilon_f' (2N_f)^c. \quad (2)$$

$\Delta \varepsilon_p$ is the plastic strain range, ε_f' and c are the fatigue coefficient and exponent respectively, and N_f is the number of cycles. This relation strictly applies only to the situation of large strain values, where plastic strain dominates. Typical values for the exponent (c) are between about -0.5 and -0.7 for most metals. A similar relation was described by Basquin [17] for the fatigue stress as function of the number of repetitions, which Morrow proposed to write [18]:

$$\sigma_a = \sigma_f' (2N_f)^b. \quad (3)$$

Here, σ_a is the fatigue strength, σ_f' and b are the fatigue strength coefficient and exponent, and N_f the number of cycles. Values for the exponent (b) are normally in the range of -0.07 to -0.12. This latter expression is also referred to as high-cycle fatigue. Morrow recognized that because stress and strain are connected through the elastic modulus (E), both equations can be combined to an expression for the total strain amplitude $\Delta \varepsilon/2$ [18]:

$$\frac{\Delta \varepsilon}{2} = \frac{\sigma_f'}{E} (2N_f)^b + \varepsilon_f' (2N_f)^c. \quad (4)$$

It thus follows that two slopes exist in a diagram of the total strain amplitude versus the number of cycles, two slopes that describe two regimes. Below about 10,000 cycles low-cycle fatigue occurs while (very) high-cycle fatigue should be found at one million cycles or more [19]. In between there is a transition region.

At several occasions in his paper on the effects of thermal stress on the cyclic durability of metals, Manson points out that concentration of stress is of great importance [16]. Whereas in brittle materials such concentration of stress determines the failure, this is not so in ductile materials – unless the stress is applied cyclically and plastic strain accumulates. This has eventually led to considering the plastic strain energy as the leading influence factor for fatigue [18]. Later, more sophisticated approaches were proposed, as one can read in the review on prediction methods for fatigue damage [20].

With respect to wearable electronics it was recognized that even at small elongations deformation can pile up and lead to failure. By means of finite element modeling the locations of maximum stress and strain in a stretched meander structure were identified. These are the apex and the inflection point in the meander [9].

We will now use the above to analyze the lifetime data on stretchable samples in section 3.2 and similar for the electronic-textile samples in section 3.3.

3.2 Lifetime modeling for stretchable technology

Turning to the actual data, Figure 17 represents the engineering strain range versus the cycle life of the stretchable test structures. Two power law curves such as equation (2) have been fitted through the data. Their exponents are for the SCB-data $c = -0.37$ and for the SMI-data $c = -0.32$. For SMI the curve was fitted through the data with the exclusion of the points at 4% and 2.6% strain.

Two remarks must be made to this analysis. In the first place, the data point for the SMI-samples at an elongation of 2.6% does not represent a failure (see Table 1) and an actual failure would thus occur after more cycles. But already there is an indication that the data point deviates from the fitted power law. This could mean that stretching to 2.6%, and perhaps already at 4%, involves mainly elastic deformation and the high-cycle regime applies. The second remark concerns the values of the exponents of the power law function. Although the values are in line with other reported values of the fatigue exponent for Cu-structures, and in particular for such of comparable thickness where values of -0.14 to -0.46 could be evaluated [21], one must be cautious as to the precise value of the exponents in view of the above mentioned effect of stress concentration. Below it will be demonstrated what the consequences are for the analyses of the test data.

In particular the work at IMEC [9] referenced in the previous subsection made clear that the highest deformation concentrates at the apex and the inflection points of the meandering Cu-trace. In our experiments the apex is indeed the position where failure occurs (see e.g. Figure 12), but no failure was observed at the inflection point. By finite element modeling the plastic strain was computed as function of the engineering strain for two PDMS-materials [9]. For a correct model description of fatigue failure that takes the actual deformation into account, not the elongation as used in Figure 17 is needed, but one must take the plastic strain. The data reported in [9] for the substrate material Sylgard 186 was used to transform the elongation that was applied in the test (see Table 1) to plastic strain. Thus, the result of Figure 18 is obtained which we show together with the initial analysis. The power law of equation (2) was fitted to the data of 5% engineering strain or higher, which gives an exponent of $c = -0.60$. This value is nearly the same as the exponent that the IMEC-paper reports of $c = -0.59$.

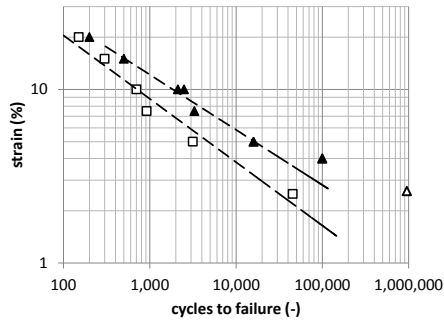


Fig. 17 Engineering strain versus cycles to failure for SCB- (□) and SMI-technology (▲) [5]. For the SMI-series at 2.6% the sample had not yet failed (△). The dashed lines are power-law fits.

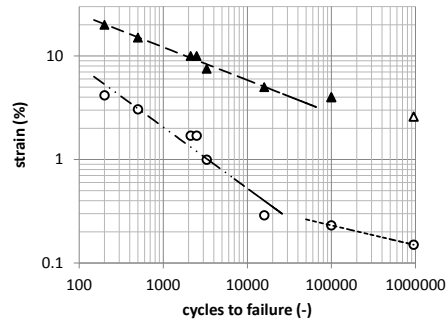


Fig. 18 Strain versus cycles to failure of SMI-test samples (same data as in Figure 17). Engineering strain (▲) and plastic strain (○) according to [9]. The lines are explained in the text.

As was explained in the introductory part of this chapter, in the case where plastic strain dominates the power law usually has an exponent in the range of -0.5 to -0.7 . The above analysis with an exponent of -0.60 is thus in good agreement. Moreover, also the failure analysis shows that failure is due to plastic deformation; see for instance the photos in Figure 11 and Figure 12.

The two data points taken at 4% and 2.6% engineering strain were not included in this analysis – from 4% and below the slope of the power-law curve is less: $c = -0.19$ (see dotted line in Figure 18), which is somewhat higher than was mentioned above for high-cycle fatigue. However, since at 2.6% no failure had occurred yet, the true power law will have a still lower value than -0.19 . This is a clear indication for the transition from low- to high-cycle fatigue.

The same procedure cannot be done for the SCB-samples since no such assessment of the plastic strain has been done yet.

3.3 Lifetime modeling for textile technology

The textile samples were not stretched but bent, and thus a different analytical approach is required. In the test, the samples were held straight by springs and in the center they were vertically displaced over a certain distance (z), see Figure 6. It is thus now necessary to derive a relation between this displacement and the bending strain. The maximum bending strain in a beam of thickness d over a radius R is:

$$\varepsilon_b = \frac{d}{2R}. \quad (5)$$

The system of the textile, the conducting yarn, and the spring can be regarded as a beam which is kept fixed at one end (A), see Figure 19. Point A is the edge of the LED-globtop combination. For bending of a beam of length l the displacement caused by the force (F) at any location (x) is given by:

$$z = \frac{Fx^2}{6EI}(3l - x). \tag{6}$$

E is the elastic modulus and I the moment of inertia of the beam. For the strain at the constrained end of the beam (A) the radius of the curve of the beam at that point must be determined. The curvature – i.e. the inverse of the bending radius – is:

$$K(x) = \frac{z''}{(1+z'^2)^{3/2}}, \tag{7}$$

where z' and z'' are the first and the second derivatives of the displacement (z , equation (6)). Working this out, we have at point A (for $x = 0$, the edge of the rigid part) that the curvature is proportional to the force which is the only variable:

$$K(0) = \frac{Fl}{EI} \propto F. \tag{8}$$

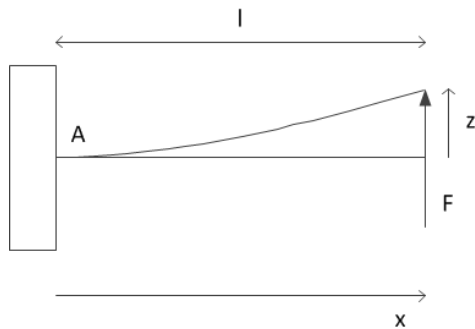


Fig. 19 Bending of a beam of length l by a force F . The beam is fixed at point A ($x = 0$).

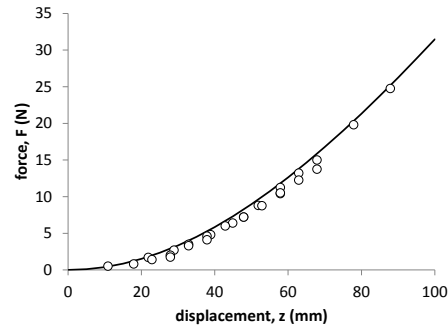


Fig. 20 Experimentally measured force-displacement of textile (\circ). Calculated force from spring constant (drawn line).

The next step is to evaluate the force as function of the imposed displacement. This was done in two ways. First, the force in the vertical direction and the resulting displacement of the test sample were measured (see Figure 6). (Note that in the actual cyclic test the sample is moved up and down by a clamp which is attached to a piston with air pressure. For this particular purpose the clamp was removed in order to only move the textile with the springs to keep it straight.) Figure 20 gives the results of force versus the displacement as the open symbols. With respect to the second assessment, we must realize that the origin of the force originates from the four springs keeping the textile straight. Referring again to the setup of Figure 6, the displacement (z) and the angle (α) determine the elongation of the springs. Together with the spring constant the force along the direction of the textile is obtained, which is also shown in Figure 20 as the drawn line.

The full expression for the force of the four springs ($F_{springs}$) and the curve-fitted relation for the measured force on the test jig (F_{jig}) are given by the following equations:

$$F_{springs} = 4k \left(\frac{z}{\sin \alpha} - l \right), \alpha = \arctan \left(\frac{z}{l} \right), \quad (9a)$$

$$F_{jig} = 0.0033z^2 - 0.0079z. \quad (9b)$$

The spring constant $k = 0.19$ Nm and the length $l = 100$ mm. Returning to the test results of Table 2, these are now complemented with the force on the textile, using equation (9b). Table 3 lists the result, and so, finally, the bending strain expressed in terms of the acting force can be plotted against the cycle life, see Figure 21. A power-law fit to the data yields an exponent of $c = -0.41$.

Table 3 Displacement (z) and observed cycles to failure for textile (see Table 2). The force (F) is calculated with equation (9b).

Textile	z (mm)	F (N)	Cycles to failure
Dtex: 76	86	23.73	25000±7000
Picks/cm: 33	77	18.96	49000±8000
	59	11.02	105000±20000
	35	3.77	1500000

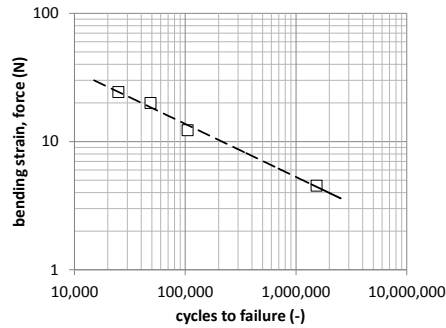


Fig. 21 Bending strain given as force (see Table 3) versus cycle life in textile sample. The fitted line is a power-law fit.

This value can be compared to the exponent that was obtained for the engineering strain of the stretchable substrates, which is in the range of -0.32 to -0.37 (see section 3.2). The difference does not seem very impressive. For the stretchable samples we were able to estimate the plastic strain, which is not yet possible for the bending of the conducting Cu-yarns in the woven textile.

But even if we do not know the plastic strain, we can summarize the analysis of the cyclic bend tests on electronic textile by concluding that the result gives confidence that the qualitative expression for the bending strain is correct.

4. CONDUCTOR NETWORKS

In the second chapter we explained that there are some special situations. Both groups of technologies contain a separate case in which the electrical conductivity evolves differently under cyclic mechanical loading than in the other cases which were treated in chapter 3.

The SPB-technology – based on non-woven materials with screen-printed conductors – differs from the SCB- and SMI-technologies. As was shown in the original paper [5], the resistance of the meandering tracks does not stay constant and upon failure suddenly increases, as happens in the two other technologies. Rather, the resistance increases gradually, and at some point it becomes irregular. Here, a typical example of a failed sample is shown in Figure 22, which indicates that the screen-printed structure breaks up because of its granular structure. The resistance was recorded during the cycles and is shown per each cycle as the value at 5% elongation and at rest. Figure 23 gives the resistance data which become irregular in the stretched state after about 200 cycles.



Fig. 22 Failure mode of SPB-sample after test to 5% stretching [5]. Cracks are visible in the screen-printed layer.

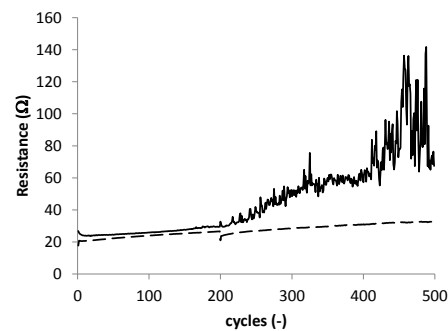


Fig. 23 Resistance of SPB-sample under cyclic stretching from 0% (dashed line) to 5% (solid line). From [5].

The second special case is the combination of two methods to apply a conducting yarn to non-woven textile substrate, as is shown in Figure 4 where a stitched and an embroidered yarn are connected by a knot. The thin silver-coating of the yarns will be damaged under mechanical loading [8] (see Figure 24). Initially, the conduction takes place through the coating of each individual filament and, because these are in direct contact in the bundle, there is also inter-filament conduction. When the coating is damaged, less intra-filament conduction is possible. But between the filaments a conducting resistor network may still exist. It lies at hand that the inclusion of a knot to connect two yarns further complicates the conductivity since the interconnection is formed by a clamped contact. This clamp loosens upon cyclic mechanical loading and in a clamped contact the resistance increases when the clamping force is reduced. Typical data are shown in Figure 25 for cyclic bending over a vertical displacement of 86 mm. At a few instances the test was interrupted, this can be seen as the decrease of the resistance at 500, 1000, 2000, and 3000 cycles. After resuming the cyclic loading the value prior to the interruptions is reached again.



Fig. 24 Failure mode of embroidered yarn on non-woven textile after cyclic bending. Damage to the Ag-coating of the filaments is visible.

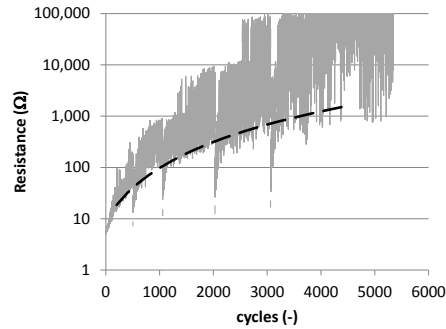


Fig. 25 Resistance of non-woven sample with knot between stitched and embroidered yarn under cyclic bending. The dashed line is explained in the text.

We thus have two super positioned effects in these measurements. First, there is the background of the gradual increase of the resistance as function of the number of stretching and bending cycles. This is the interpretation of the dashed line in Figure 23 for stretchable SPB-substrates which reflects the sample at 0% elongation for each cycle. Very tentatively, that gradual increase of the resistance is attributed to reduction of the elasticity of the substrate material which functions to keep the conducting Ag-particles in tight contact. For the non-woven sample no data were taken at the exact moments that the sample was in the un-stretched state, therefore we have indicated the background with the dashed line in Figure 25. The clamping force of the knot-interconnection stems from the stitching and embroidering which force loses strength. The second effect adds to the background resistance. This appears as an increasing and significant variation of the resistance during mechanical cycling which is further discussed below.

In the two situations, it is very likely that the large variation of the resistance is caused by percolation. Percolation theory describes the behavior of clustered elements with a certain physical functionality, such as electrical conduction (e.g. for instance [22]). One considers a network composed of sites that can be occupied by one element, with a probability p that the site is occupied. If two adjacent sites are occupied, the transport process takes place between them. In the network conduction is possible when there is at least one coherent cluster of occupied sites between the two ends of the network, i.e. the contacts to the conducting track or yarn. Below the critical probability that a site is occupied – the so called percolation threshold p_c – the conduction vanishes. Close to this value the conduction (Σ) is described by [23]:

$$\Sigma \propto (p - p_c)^t. \quad (10)$$

The value of the critical site occupancy p_c and the exponent t depend on various factors, such as the dimensionality of the system. Typically, one reports values of $p_c = 0.25-0.5$ and $t = 1.5-2$ [22, 23, 24].

The elements to occupy a site in case of the two types of test structures are the Ag-flakes of the screen printed conductor in the SPB-samples, and the conducting yarns with Ag-coating in the non-woven textile samples. Both form a conductor network. The bottom line of this expose is that at some point the connected cluster of conducting elements reaches the percolation threshold. The probability of site occupancy approaches $p = p_c$. Even small variations in the number and strength of the bonds between the elements will then have large impact on the resistance, as one sees in Figure 23 and Figure 25 and which follows from equation (10). In particular in the stitched interconnection the resistance varies per bend cycle over two orders of magnitude.

To summarize, under cyclic mechanical loading, the conductivity in systems made with screen-printed particles or with clamped conducting yarns decays by two mechanisms. On the one hand one has a declining clamping force that leads to gradually increasing resistance. On top of this, the electrical contacts between conducting particles and yarns become less and less in number, which leads to the formation of a percolation network with unstable conductivity.

5. SUMMARY AND CONCLUSIONS

In this contribution no new data were presented. Instead, existing results from two projects on wearable electronic applications and technologies have been reviewed and attempts have been made to refine the originally reported analyses. To this end we used analytical models to come to a qualitative description of the bending strain of conducting yarns in electronic textiles. The bending strain is proportional to the force that is used to keep the textile straight in the test. The cycle life obeys a power law with an exponent that compares well with the one found for the cycle life of the stretchable substrates.

As to the stretchable substrates, for the SMI-technology the engineering strain was transformed to plastic strain values using results from finite element simulations that were carried out elsewhere. As a result the power-law dependence is better in agreement with low-cycle fatigue.

These evaluations show where still work needs to be done. In particular, modeling of the plastic strain that accumulates in the cyclic bend test for electronic textiles is such a topic.

Finally, an additional failure mechanism has been observed in clamped contacts. In some subsets of the stretchable and textile technologies, the contact force between conducting particles or between conducting yarns gradually diminishes, which might be attributed to fatigue. But eventually a conductor network evolves that behaves as a percolation network. This is also a topic that may receive further attention.

Acknowledgement. *Instead of mentioning each individually, the author would like to thank all colleagues that contributed to the STELLA and PLACE-it projects and who have supplied him with additional information for this paper. Co van Veen's critical reading of the text is greatly appreciated.*

REFERENCES

- [1] T. Löher, M. Seckel, R. Vieroth, C. Dils, C. Kallmayer, A. Ostmann, R. Aschenbrenner, H. Reichl. *Stretchable electronic systems: realization and applications*. Proc. 11th EPTC, 2009, pp 893–898.
- [2] B. Schmied, J. Guenther, C. Klatt, H. Kober, E. Raemaekers. *STELLA – stretchable electronics for large area applications*. Adv. Sci. Technol. 2008, vol. 60, pp 67–73.
- [3] F. Bossuyt, T. Vervust, F. Axisa, J. Vanfleteren. *Improved stretchable electronics technology for large area applications*. Proc. MRS spring meeting symposium, 2010, pp 1271–1277.
- [4] K.H. Cherenack, L. van Pieteron. *Smart textiles: challenges and opportunities*. J. Appl. Phys. 2012, vol. 112, no 9, 091301.
- [5] F. Bossuyt, J. Guenther, T. Löher, M. Seckel, T. Sterken, H. de Vries. *Cyclic endurance reliability of stretchable electronic substrates*. Microelectronics Reliability, 2011, vol. 51, pp 628–635.
- [6] M. Jablonski, R. Lucchini, F. Bossuyt, T. Vervust, J. Vanfleteren, H. de Vries, P. Veau, M. Gonzalez. *Impact of geometry on stretchable meandered interconnect uniaxial tensile extension fatigue reliability*. Microelectronics Reliability, 2014, accepted for publication.
- [7] H. de Vries, K.H. Cherenack. *Endurance behavior of conductive yarns*. Microelectronics Reliability, 2014, vol. 54, pp 327–330.
- [8] M. de Kok, H. de Vries, K. Pacheco, G. Van Heck. *Reliability of conducting yarns in electronic-textile applications*. Textile Research Journal, 2014, submitted.
- [9] M. Gonzalez, F. Axisa, M. Vande Broucke, D. Brosteaux, B. Vandeveldel, J. Vanfleteren. *Design of metal interconnects for stretchable electronic circuits*. Microelectronics Reliability, 2008, vol. 48, pp 825–832. M. Gonzalez, F. Axisa, F. Bossuyt, Y.Y. Hsu, B. Vandeveldel, J. Vanfleteren. *Design and performance of metal conductors for stretchable electronic circuits*. Proc. 2nd ESTC, 2008, pp 371–377.
- [10] D.H. Kim, J.A. Rogers. *Stretchable electronics: materials strategies and devices*. Adv. Mater. 2008, vol. 20, pp 4887–4892.
- [11] F. Bossuyt, T. Vervust, J. Vanfleteren. *Stretchable electronics technology for large area applications: fabrication and mechanical characterization*. IEEE Trans. Comp. Pack. Manuf. Technol. 2013, vol. 3, no. 2, pp 229–235.
- [12] M. Jablonski, F. Bossuyt, J. Vanfleteren, T. Vervust, H. de Vries. *Reliability of a stretchable interconnect utilizing terminated, in-plane meandered copper conductor*. Microelectronics Reliability, 2013, vol. 53, pp 956–963.
- [13] M. Jablonski, R. Lucchini, F. Bossuyt, T. Vervust, J. Vanfleteren, H. de Vries, P. Vena, M. Gonzalez. *Impact of geometry on stretchable meandered interconnect uniaxial tensile extension fatigue reliability*. Microelectronics Reliability, 2014, submitted.
- [14] Y.Y. Hsu, B. Dimic, M. Gonzalez, F. Bossuyt, J. Vanfleteren, I. De Wolf. *Reliability assessment of stretchable interconnects*. Proc. IEEE IMPACT, 2010, pp 1–4; *Polyimide-enhanced stretchable interconnects: design, fabrication, and characterization*. IEEE Trans. Electron Dev. 2011, vol. 58, no. 8, pp 2680–2688.
- [15] H. de Vries, K.H. Cherenack. *Failure modes in textile interconnect lines*. IEEE Electron Dev. Lett. 2012, vol. 33, no. 10. Pp 1450–1452.
- [16] S.S. Manson. *Behavior of materials under conditions of thermal stress*. NACA TN 2933, 1953. L.F. Coffin Jr. *A study of the effects of cyclic thermal stresses on a ductile metal*. Trans. ASME 1954, vol. 76, pp 931950.
- [17] O.H. Basquin. *The exponential law of endurance tests*. Proc. ASTM 1910, vol. 10, pp 625–630.
- [18] J.D. Morrow. *Cyclic plastic strain energy and fatigue of metals*. ASTM STP 1965, vol. 378, pp 45–87.
- [19] S.S. Manson. *Thermal stress and low-cycle fatigue*. New York: McGraw-Hill, 1966.
- [20] A. Fatemi, L. Yang. *Cumulative fatigue damage and life prediction theories: a survey of the state of the art for homogeneous materials*. Int. J. Fatigue 1998, vol. 20, nr. 1, pp 9–34.
- [21] D. Farley, Y. Zhou, F. Askari, M. Al-Bassyouni, A. Dasgupta, J.F.J. Caers, H. de Vries. *Copper trace fatigue models for mechanical cycling, vibration and shock/drop of high-density PWAs*. Microelectronics Reliability 2010, vol. 50, pp 937–947 .
- [22] D. Stauffer. *Introduction to percolation theory*. Taylor & Francis, 1985.
- [23] J.P. Clerc, G. Giraud, J.M. Laugier, J.M. Luck. *The electrical conductivity of binary disordered systems, percolation clusters, fractals and related models*. Adv. Phys. 1990, vol. 39, nr. 3, pp 191–309.
- [24] M. Cattani, M.C. Salvadori, F.S. Teixeira. *Insulator-conductor transition: a brief theoretical review*. 2009, arXiv:0903.3587.